Rock and Soil Mechanics 2026 47(1): 101−114 ISSN 1000−7598
https: //doi.org/10.26599/RSM.2025.94300110 journal homepage: rocksoilmech.whrsm.ac.cn

Evolution of damage and permeability characteristics in roadways under mining disturbance

YANG Yun-qin, HAN Li-jun

State Key Laboratory of Intelligent Construction and Healthy Operation and Maintenance of Deep Underground Engineering, China University of Mining and Technology, Xuzhou, Jiangsu 221000, China

Abstract: The mining works in underground coal mines induce the changes in stress state of rock mass in front of mining face, which can lead to rock mass damage, form groundwater seepage channel, and then cause disasters such as water inrush and surrounding rock collapse. In view of this situation, three stress loading paths are designed to simulate the stress state of rock mass under mining disturbance in different regions: conventional triaxial compression test(CTCT), loading axial pressure and unloading lateral pressure test(IUT), and keeping axial pressure and unloading lateral pressure test(KUT) for triaxial compression tests, and creep tests of two loading modes are designed: the creep test involving step loading and unloading confining pressure are conducted to investigate the evolutionary characteristics of rock damage and permeability and their time-dependent mechanisms. The damage to limestone during creep and creep unloading processes is characterized through theoretical analysis. The results show that:(1) Limestone exhibits significant differences in mechanical and permeability properties, such as yield characteristics and permeability, under different stress paths. However, shear failure dominates its failure mode in all cases. (2) As confining pressure gradually increases, the stress paths corresponding to the maximum permeability growth rate are CTCT, IUT, and KUT respectively. This indicates that the evolution of limestone permeability is closely related to in-situ stress levels and stress states. (3) Damage primarily occurs during axial loading and confining pressure unloading processes. The rate of damage accumulation and failure in limestone is faster under confining pressure unloading paths than under conventional loading paths. (4) A modified Nishihara model was developed, and its reliability was successfully validated. The research results can provide reference for the construction stability research in underground engineering, such as roadways and tunnels.

Keywords: mining disturbance; damage; mechanical properties; permeability characteristics; patterns of evolution

1 Introduction

In the mining engineering of underground mine, the mining disturbance caused by construction and the seepage of groundwater are the important reasons for the deformation and instability of roadway surrounding rock. With the increase of mining intensity and depth of underground mine, the problems caused by water inrush and collapse have become the major problems restricting the efficient and safe mining of underground mine[1-3]. Due to the inconsistent disturbance of rock mass caused by different construction conditions, many scholars[4-8] put forward the concept of stress path to study the characteristics of rock mass under different working conditions. The underground rock mass is in a three-dimensional stress state, in which the vertical stress is the maximum principal stress for some rock masses, and the horizontal stress is the maximum principal stress for some rock masses, and the direction of the principal stress will significantly affect the performance of rock mass[9, 10]. Therefore, the ratio of vertical stress to horizontal stress λ (lateral pressure coefficient) is defined. These two stress states are described by the magnitude relationship between the value and 1[11]. In addition, in the excavation of roadway or tunnel in underground engineering, it is also necessary to pay attention to the relationship between the direction of excavation and the direction of principal stress, so as to minimize the disturbance and damage to strata[12].

Conventional triaxial compression test(CTCT) is a commonly used method to test rock mass performance. In the test, confining pressure is usually kept constant, and axial pressure is used as the maximum principal stress, which is different from the condition $\lambda>1$. In addition, the excavation of rock mass is a process of unloading, and the performance of rock mass is also different during loading and unloading[13-15]. Previous studies have shown that the difference between loading and unloading has little impact on rocks with large elastic modulus and high stiffness[16]. However, for most rock masses, there are significant differences in constitutive relationship, failure mechanism and performance evolution[17].

In the research of rock mass damage, it is generally believed that there are two thresholds: the threshold of damage generation and the threshold of damage destruction. For brittle rocks, in the process of damage evolution, when the loading reaches 30%-50% of the

Received: 22 February 2025 Accepted: 01 July 2025
First author: YANG Yun-qin, male, born in 1998, PhD candidate, focusing on rock mechanics and underground mining stability. E-mail: yyq265012@163.com
Corresponding author: HAN Li-jun, male, born in 1966, PhD, Professor, research interests: rock mechanics and engineering stability, geotechnical support and reinforcement. E-mail: hanlj@cumt.edu.cn

uniaxial compressive strength, damage begins to occur inside the rocks, and when the loading reaches about 80%, macroscopic damage occurs[18-19]. The identification of these two thresholds can be achieved through the energy-dissipation method[20-22], which is also applicable to deep coal rock, etc.[23] and can be used for the stability analysis of surrounding rock[24]. Some scholars further proposed a prediction method for damage generation and development depth during tunneling based on these two thresholds[25], and verified the consistency of the threshold theory with actual rock mass performance through Renormalization Group theory[26]. The above tests on rock mass damage all show that the development of damage generally stops after the loading peak, and the morphology of damage cracks is affected by rock inhomogeneity[27]. In terms of rock mass damage monitoring, acoustic emission(AE) technology has been widely applied to rock mass damage detection under different conditions[28-29]. In terms of damage characterization, the ratio of a certain property between damaged rock mass and intact rock mass is commonly used to characterize the damage degree, that is, the damage factor[30]. Some scholars also found that the radial strain value at peak loading is insensitive to pore water pressure and rock anisotropy, and it is proposed as a condition-insensitive damage indicator of rock in creep tests[31]. This conclusion can also provide reference for the related research of rock mass permeability.

With the advancement of research for many years, seepage channels[32-33], fluid particles[34], variable mass seepage[35] and other factors have been gradually introduced into the research, and the understanding and cognition of seepage in rock mass has gradually transitioned from linear flow to nonlinear flow. The assumption of continuous rock mass is gradually transformed into a discontinuous assumption considering the existence of soil matrix[36], but the difference between the two is believed to gradually decrease with the extension of seepage time[37]. Considering the influence of disturbance, it is mainly reflected in the development of damage of underground rock mass under the action of disturbance. With the expansion of cracks, the seepage mode transitions from pore flow to fracture flow, and even finally forms pipeline flow[38]. However, there is a threshold for the damage evolution of rock pores in the process of cyclic disturbance, beyond which the permeability can be significantly affected[39]. On the whole, permeability is negatively correlated with confining pressure[40].

For coal mining, the stress state of the rock mass will undergo different changes due to the tunneling of the working face, thereby causing different forms of damage and having different influences on the seepage characteristics of the rock mass. The above-mentioned studies mainly focus on the rock mass damage caused by regional single stress states and the seepage characteristics after the damage occurs. The test methods adopted are relatively simple, and there are relatively few studies on the mechanism of timeliness. Therefore, this paper will address this scientific issue, simulate different rock mass disturbance conditions through various test methods and different stress loading paths, consider the damage evolution and time effect in the stress-seepage coupling process, study the evolution of the mechanical and permeability characteristics of the rock during the disturbance process, and make improvements based on the existing creep constitutive model to characterize the disturbance process of the rock mass.

2 Research method

2.1 Material

The sampling site is -700 m level of a coal mine in western Henan Province. The sample was drilled by the hydrodrill method and prepared into a cylinder with a diameter of 50 mm and a height of 100 mm. The sample preparation process was carried out according to the International Society of Rock Mechanics (ISRM) standard[41]. The height error of the sample was not more than 0.28 mm, the end face was perpendicular to the axis, and the deviation was within 0.2°.

2.2 Experimental plan and experimental system

In essence, roadway excavation is a lateral unloading process of rock mass[14], and the change of its vertical stress (abutment pressure) is affected by the change of distance from the excavation face, as shown in Fig.1. In the figure, K is the lateral pressure coefficient, γ is the weight of the overlying rock mass, H is the burial depth, and σ_y is the vertical stress With the advance of the working face, the abutment pressure of the rock mass also moves forward. The stress state of the rock mass in the pressurized zone (region B) is shown in Fig.1(a), which is characterized by the reduction of confining pressure (σ_3) due to driving and unloading, and the increase of axial pressure (σ_1) due to the advance of the working face, and it is always greater than the stress of the original rock. The stress state of rock mass in the transition zone is shown in Fig.1(b). Due to the long distance from the working face, σ_1 of this part of rock mass is gradually stable. In fact, σ_3 is also relatively stable in the pressurized zone. The stress state of rock mass in the stable pressure zone (region C) is shown in Fig.1(c). Both σ_1 and σ_3 remain stable due to the distance from the working face.

There are three triaxial loading schemes for limestone in total, as shown in Fig.1(d). The average measured horizontal stress at the sampling site is about 17.5 MPa, so the predetermined σ_c values taken in the test are 5, 10 and 20 MPa. The seepage pressure refers to the water pressure at a certain position at this level, which is 3 MPa. Before the test, all samples were saturated with water, and the specific loading scheme was as follows:

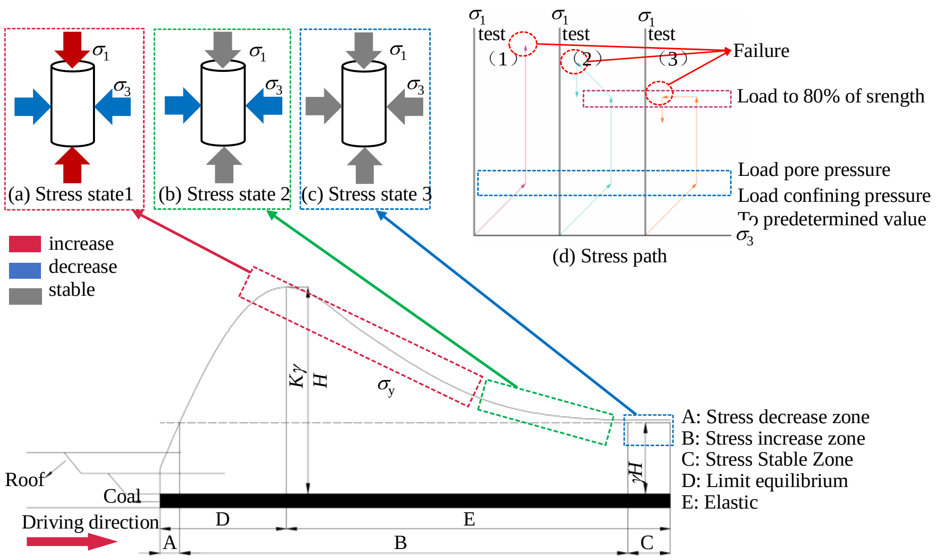

Fig.1 Stress distribution ahead of working face and the corresponding test stress path

Test (1) is a conventional triaxial compression test(CTCT). First, the σ_c is loaded at a rate of 0.05 MPa/s, and the osmotic pressure is loaded after reaching a predetermined value, and the state is maintained for 24 h. After σ_3 is kept unchanged, the σ_1 is loaded at a rate of 0.002 mm/s. After the specimen is broken, the σ_1 is controlled by displacement loading until it does not change with the axial strain.

Test (2) simulates the stress state in Fig.1(a), namely increasing axial pressure and unloading confining pressure(IUT). First, the σ_3 is loaded at a rate of 0.05 MPa/s, and the seepage pressure is loaded after reaching a predetermined value, and the state is maintained for 24 h. After that, σ_1 is loaded to 80% of the peak strength obtained in test (1) at a rate of 0.05 MPa/s, and the state is maintained for 2 h. Then, σ_1 is loaded and σ_3 is unloaded at a rate of 0.05 MPa/s. After the specimen is damaged, σ_3 remains unchanged, and the σ_1 is controlled by displacement loading. The evolution characteristics of permeability in the post-peak stage was measured.

Test (3) simulates the stress state in Fig.1(b), namely keeping axial pressure and unloading confining pressure (KUT). Different from test 2, after loading σ_1 to 80% of the peak strength obtained in test 1and maintaining the state for two hours, σ_1 is kept unchanged, and σ_3 is unloaded at a rate of 0.05 MPa/s. After failure, σ_3 is kept unchanged, and the axial pressure is controlled by displacement loading to measure the evolution characteristics of permeability in the post-peak stage of the sample.

The creep test is also carried out in accordance with two loading methods, and the specific scheme is as follows:

The creep test (1) is carried out by step loading. After the predetermined confining pressure is applied, seepage pressure is applied at the upper end of the sample, and negative pressure is applied at the lower end. Each level of axial load is loaded at the rate of 0.05 MPa/s, and the next level of load is loaded when the axial strain rate reaches 3‰ until the sample is damaged.

In creep test (2), the confining pressure is first loaded to a predetermined value at a rate of 0.05 MPa/s. Considering that the creep test of unloading σ_3 has certain requirements for the initial level of confining pressure, the initial values of confining pressure are set as 10 MPa and 20 MPa. σ_1 is loaded at a rate of 0.05 MPa/s to 80% of the average peak strength obtained in test 1. At this time, the pore water pressure above the sample is 3 MPa, the lower surface of the sample is connected with atmospheric pressure (as shown in Fig.2), and the sample is maintained in this state for 24 h to achieve seepage equilibrium. The creep test is carried out and the permeability and strain evolution are recorded. The creep at this stage is maintained for about 4000 min. After that, σ_1 remains unchanged, and σ_3 is unloaded at a rate of 0.05 MPa/s. When the value of σ_1 decreases significantly, the unloading of σ_3 is stopped.

The experimental system used in this experiment is shown in Fig.2, including seepage, mechanical loading and AE monitoring module.

The seepage system uses distilled water as the seepage medium. The water pressure on the upper surface of the rock sample is loaded by a pressure pump. The pressure gauge shows the loading pressure value. The pressure pump can keep the pore water pressure stable according to the feedback from the sensor, with an error of ±0.05 MPa, as shown in Fig.2 (a). In addition, to ensure that the water pressure is evenly applied to the upper surface of the specimen, upper and lower loading heads with annular patterns were fabricated, as shown in Fig.2 (b). During the test, the pressure heads were sealed from the sample through a heated shrink tube. During the test, the flow rate passing through the sample is detected by the sensor at the bottom of the sample, and the permeability is automatically calculated by the software.

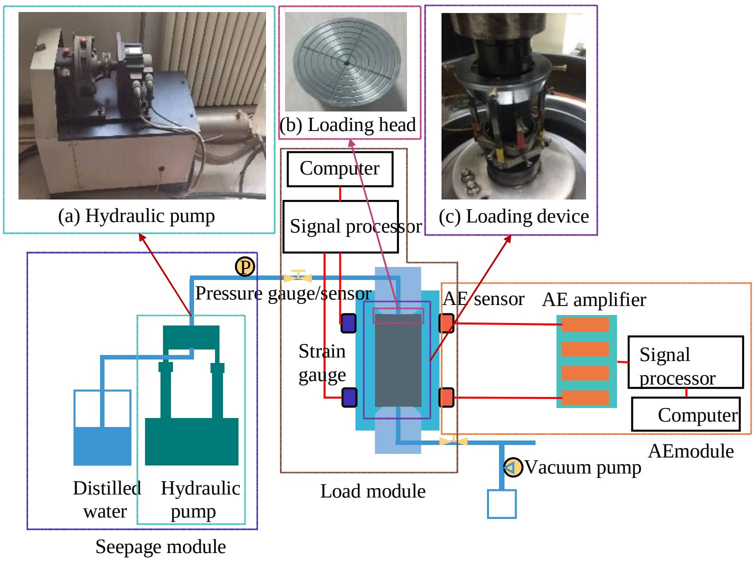

(d) Mechanical test system and AE monitoring device

Fig.2 Experimental system

The loading module is mainly based on TAW-2000 test system, which consists of axial pressure control system, confining pressure loading system, etc. The loading process is controlled by electro-hydraulic servo valve. In order to study the influence of different construction stress disturbances on rock damage and permeability characteristics, triaxial compression tests and creep tests with different stress/loading and unloading paths are designed. The specific loading modes are shown in Fig. 1(d).

The loading module used in the test does not have the function of AE monitoring itself, so an external AE monitoring module is needed. Because the confining pressure in the test is achieved by oil pressure, the AE probe cannot directly contact with the rock sample, so the AE probe is arranged outside the cylinder, and the coupling effect between the sensor and the cylinder is enhanced by petroleum jelly.

To ensure the reliability of the test results and reduce the errors caused by the discreteness of the samples, at least three samples were tested in each group of the test groups under the same conditions.

3 Results and discussion

3.1 Triaxial compression test

Triaxial compression tests of three stress paths were carried out in this study, and the results are as follows:

3.1.1 Conventional triaxial compression test

The test results of the limestone under different confining pressures are shown in Fig. 3. In addition, the loading process of the limestone is analyzed in sections according to the characteristics of the phenomena, stress-strain relationship, permeability properties and the number of AE events(N_{AE}) in the test.

Fig.3(b) shows the evolution of the distribution of AE events during the loading process of limestone specimens under confining pressure of 5 MPa. It can be seen that after the loading reaches its peak, the stress rapidly decays, which is consistent with the characteristics of brittle rocks. Therefore, the distribution of AE events when the stress is loaded to a certain stage during the test is listed according to the research of Asemi, et al.[42], as shown in Fig.3(a). It can be seen that when the loading reaches 80% of the peak intensity, N_{AE} increases significantly, accompanied by the emergence of macroscopic cracks, which is basically consistent with the research results of Cai et al.[19]. Under each level of confining pressure , the final failure form of specimens is mainly inclined shear failure, and the failure form is consistent with the distribution state of AE events. With the increase of σ_c, the closure degree of macroscopic cracks of specimens is higher. The loading process is divided into three stages as shown in the Fig.3(b): (1) In the first stage, the stress is gradually loaded, N_{AE} is very small, and the permeability coefficient gradually decreases with the loading. Considering that the permeability coefficient is directly related to the pore structure (porosity) of the rock, it can be considered that this stage belongs to the compaction stage, and the pore structure of the rock is squeezed under the external load, and the end of this stage is characterized by the permeability coefficient reaching the minimum value. At this time, the load is about 0.8σ_m, where σ_m represents the peak strength; (2) In the second stage, the loading of the specimen gradually reaches the peak value, and N_{AE} synchronously reaches the peak value, while the permeability coefficient gradually increases. After the specimen was damaged, the stress and N_{AE} gradually decreased, but the permeability coefficient still maintained an increasing trend and reached the maximum value. This stage can be considered as the failure stage, which is characterized by the maximum permeability coefficient, indicating the failure of rock mass. (3) After the failure of the specimen, due to factors such as confining pressure and the structure of the rock itself, there

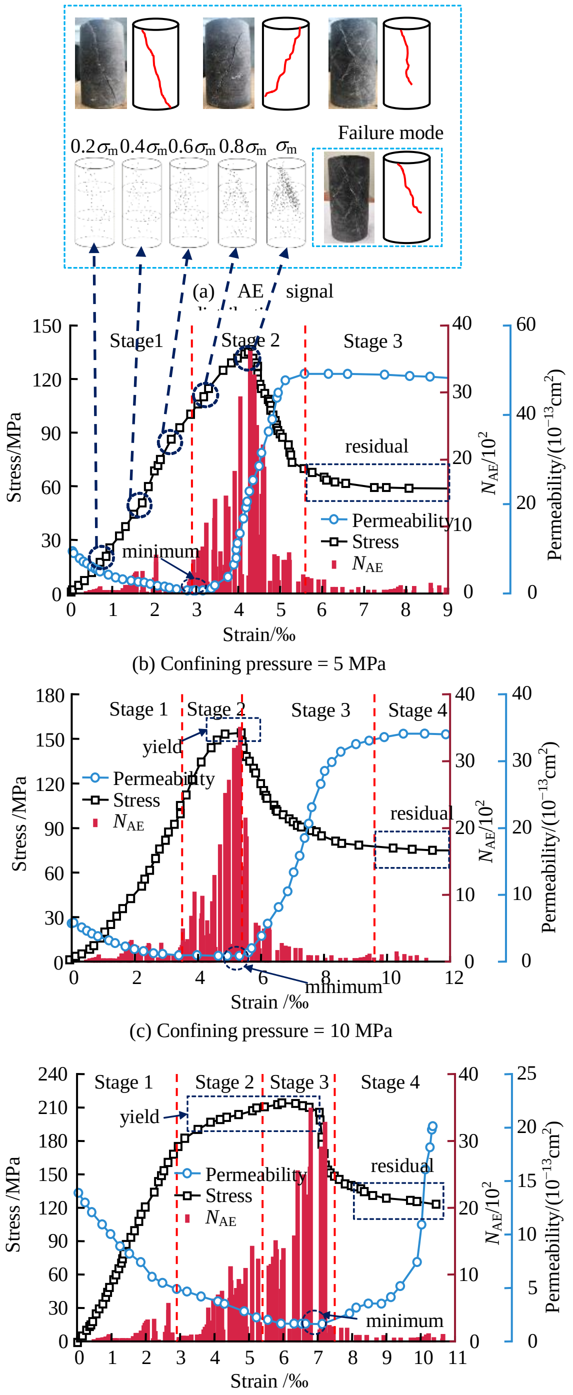

Fig.3 Mechanics, permeability and damage evolution behavior of limestone in CTCT

is still a certain bearing capacity, which can be called the residual stage, characterized by the specimen reaching the residual strength. In this stage, the permeability coefficient and stress remain stable, and N_{AE} is very small, which can be considered to be basically caused by the sliding of the internal fragments of the specimen, and the overall failure no longer occurs.

The test results under the confining pressure of 10 MPa are shown in Fig.3(c). The loading process can be divided into four stages: (1) The first stage is also the compaction stage, which is similar to the conditions under the confining pressure of 5 MPa; (2) In the second stage, due to the increase of confining pressure, a yield stage appears after the loading approaches the peak, which is manifested as constant stress and increased strain. The number of AE events rises and peaks at the time of destruction. The permeability coefficient remains at a relatively stable level and slowly reaches the minimum value, indicating that the pore structure of the sample is relatively stable during the yield stage. Compared with the evolution characteristics of stress and AE, it can be seen that the change of the permeability coefficient lags behind the damage and destruction of the rock mass, which may be due to the change of the seepage path, resulting in the change of the permeability coefficient cannot be immediately fed back to the sensor. (3) The third and fourth stages are similar to the 5 MPa condition, both belonging to the failure stage and the residual stage.

The test results under 20 MPa are shown in Fig.3(d). The loading process is also divided into four stages, and there are two notable phenomena: (1) As the confining pressure increases again, the sample exhibits a longer yield stage, which is similar to the phenomenon in Xu et al. 's tests on black sandstone and marble[43]. (2) When the sample reaches the residual stage, the permeability coefficient maintains a higher rate and reaches the maximum value, which is different from the phenomenon that the permeability coefficient of the sample at the residual stage remains relatively stable under low confining pressure. The reasons for these two points should be related to the increase of confining pressure: large confining pressure restricts the expansion of cracks in the sample, that is, the expansion of cracks is delayed at the original location of damage or even destruction, showing a certain ductility (yield stage), and the growth of permeability is therefore limited.

In addition, it can be seen that when the confining pressure is low, the minimum permeability value appears before the loading peak. With the increase of confining pressure, the minimum permeability gradually moves backward and appears after the loading peak.

3.1.2 Increasing axial pressure and unloading confining pressure test

In the stress loading path, when the axial pressure is loaded to 80% of the average strength obtained in test (1), the confining pressure begins to be unloaded while the axial pressure is loaded, and the results are shown in Fig.4.

Fig.4(b) shows the test results of the initial confining pressure of 5 MPa. The loading process can be divided into three stages, which are similar to the characteristics of the CTCT under the same confining pressure and can be divided into: compaction stage, failure stage and residual stage. The distribution and evolution of AE events during the experiment is shown in Fig.4(a). It can be seen that N_{AE} increases significantly when the load reaches 60% of the peak intensity, and macro damage occurs when the load reaches 80%. When the confining pressure is low (5 MPa), the failure form is tensile failure, which is different from that in CTCT. With the increase of confining pressure, the shear failure is gradually transformed into inclined plane shear failure, and the degree of macroscopic damage is intensified.

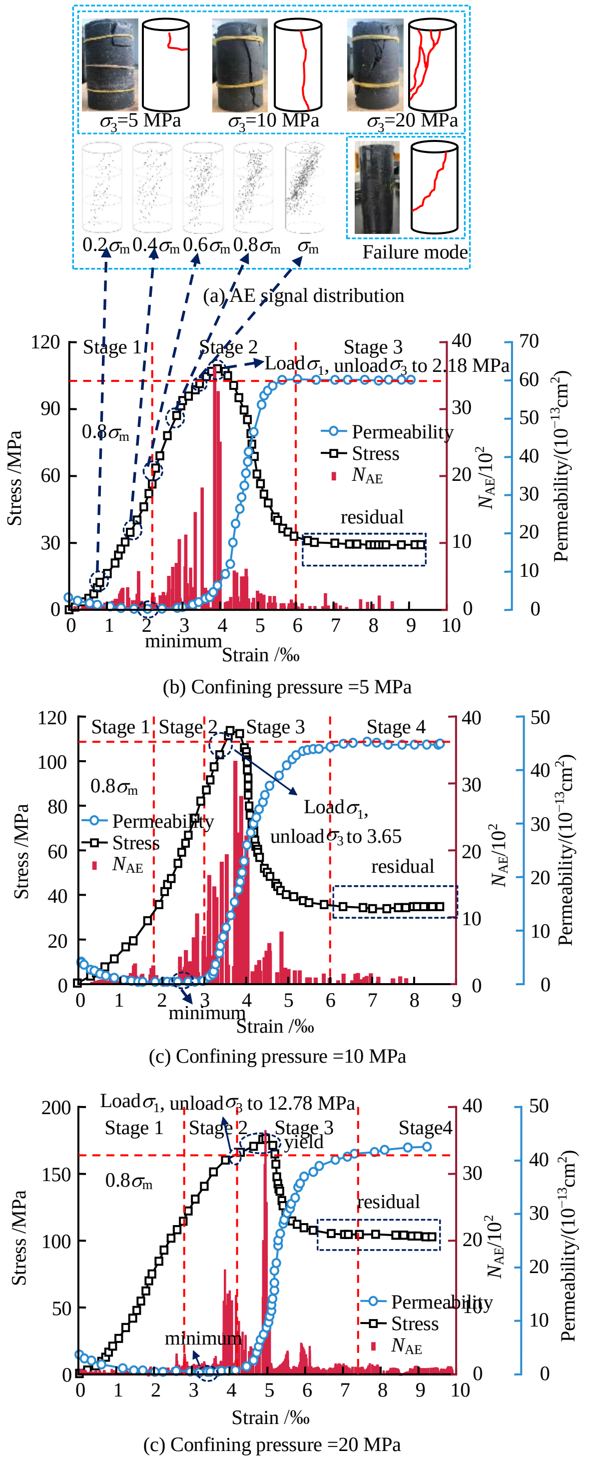

(a) AE signal distribution

(b) Confining pressure =5 MPa

(c) Confining pressure =10 MPa

(c) Confining pressure =20 MPa

Fig.4 Mechanics, permeability and damage evolution behavior of limestone in IUT

Figures 4 (c) and 4 (d) present the test results at the initial confining pressure of 10 MPa and 20 MPa respectively. The division of the loading stages is similar to that in the CTCT and can both be divided into four stages. Compared with the low confining pressure condition, the yield stage can be clearly observed, further indicating that limestone exhibits ductility characteristics in a high in-situ stress environment. After experiencing yield fatigue, the permeability coefficient of limestone still shows a certain increase in the final residual stage, which is also related to the fact that the high confining pressure limits the deformation and damage of the specimens and the propagation of cracks.

3.1.3 Keeping axial pressure and unloading confining pressure test

In the stress loading path, when the axial pressure is loaded to 80% of the average strength obtained in test 1, the axial pressure is kept unchanged while the confining pressure is unloaded, and the results are shown in Fig.5.

Under this stress loading path, the evolution characteristics of the performance of the sample is quite different from that under the stress path of test 1. The loading under different levels of confining pressure can be divided into four stages: (1) the compaction stage, whose characteristics are basically consistent with the first two kinds; (2) In the second stage, the permeability is stable near the minimum value, and the axial pressure in this stage continues to load and reaches the predetermined value, entering the third stage; (3) In the third stage, when the axial pressure reaches a predetermined value, it can be observed from Fig. 5(a), 5(b) and 5(c) that when the confining pressure begins to unload, the number of AE events rapidly reaches the maximum and the permeability begins to increase. Compared with the changes in the stress and the number of AE events analyzed above Sections 3.1.1, the change of the over-permeability has a certain degree of lag. Therefore, it can be considered that at the beginning of this stage, the sample has already produced macroscopic damage. The distribution of AE events in the loading process is shown in Fig.5(a), and its failure characteristics are also inclined plane shear failure. After that, the axial pressure is kept stable and the confining pressure is unloaded. In the process, the number of AE events decreases, but still maintain a relatively high level, and the permeability increases rapidly and reaches the maximum value. (4) In stage 4, the sample shows the characteristics of residual strength, and the permeability is stable near the maximum value.

In the test of the stress path, the confining pressures were unloaded to 2.66, 4.81 MPa and 12.62 MPa respectively. As the axial pressure was kept stable, the curve characteristics were similar to those of the yield stage, but in fact, it was only a direct reflection of the stress path and did not mean that the sample showed yield characteristics.

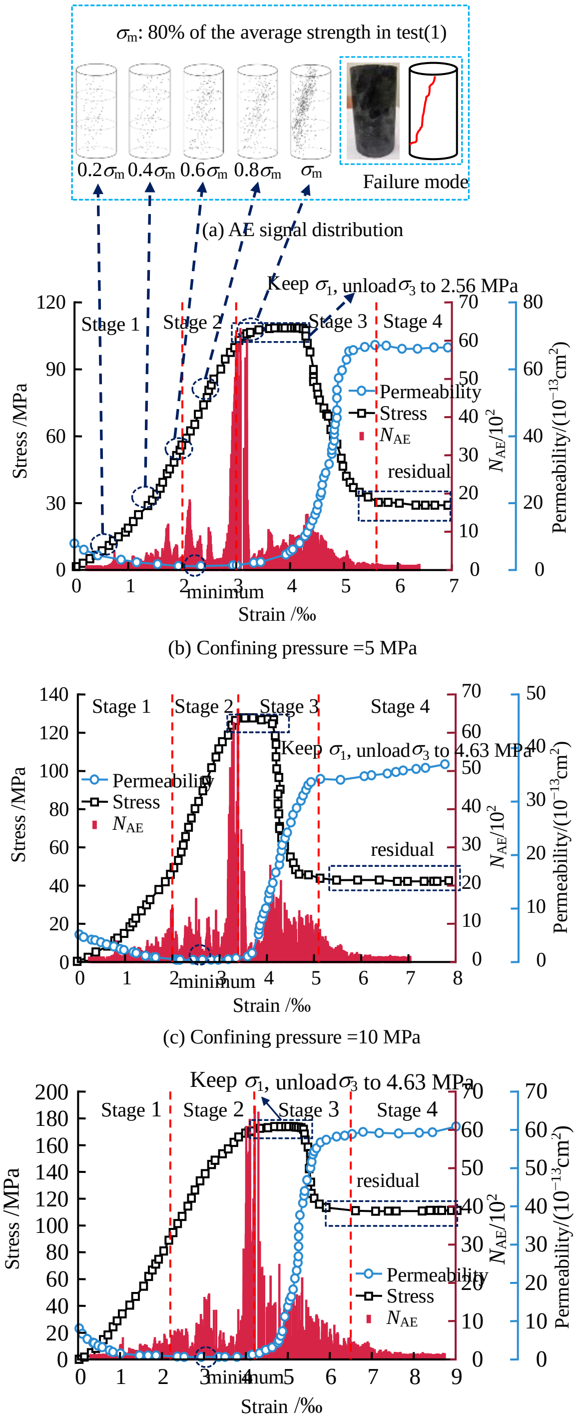

(a) AE signal distribution

(b) Confining pressure =5 MPa

(c) Confining pressure =10 MPa

(c) Confining pressure =20 MPa

Fig.5 Mechanics, permeability and damage evolution behavior of limestone in KUT

In addition, under the three confining pressure levels, when the confining pressure begins to unload, the sample immediately breaks down, which is manifested as a surge in the number of AE events. Considering the size and shape effects of the rock mass, when the long axis of the rock mass is consistent with the direction of the major principal stress, the transient damage effect of the disturbance of the small principal stress on the rock mass is considered. It is consistent with the conclusion that the unloading of small principal stress can cause transient damage by Wang et al.'s numerical simulation[44]. However, it can also be seen that in this state, the sample still maintains stability for a period of time until the deformation increases and failure occurs, which is obviously different from the rapid failure after the damage caused by large principal stress.

3.1.4 Comparison of three experiments

To explore the reasons for the differences in mechanical and permeability properties in different tests, based on the relevant theories of rock mechanics[45], for the loading path, the analysis was conducted through the average principal stress p and the generalized shear strength q:

$$p=\frac{\sigma_1+2\sigma_3}{3} \tag{1}$$

$$q=\sqrt{3J_2}=\sqrt{\frac{(\sigma_1-\sigma_2)^2+(\sigma_2-\sigma_3)^2+(\sigma_3-\sigma_1)^2}{2}} \tag{2}$$

where J_2 is the second invariant of deviatoric stress; σ_2 is One of the horizontal stresses under true triaxial stress state, orthogonal to σ_3.

Under the experimental conditions of this study, it can be simplified as:

$$q=\sigma_1-\sigma_3 \tag{3}$$

The slope of the p-q curve is defined as α, which is related to the failure mode of the material: when α<0, the material tends to undergo tensile failure (such as triaxial elongation tests); When α=0, it represents the hydrostatic pressure. For compressible soil, the main mechanical response characteristic is volume compression. When α>0, the material tends to undergo shear failure (such as in CTCT). In the three experiments of this study, the loading rates of σ_1 and σ_3 during the same loading/unloading process were the same and remained constant, Therefore, there is

$$k_{\mathrm{CTCT}}=\frac{\Delta q}{\Delta p}=\frac{\Delta\sigma}{\frac{1}{2}\Delta\sigma}=3 \tag{4}$$

$$\left.\begin{aligned}
&k_{\mathrm{IUT}}=\frac{\Delta q}{\Delta p}=\frac{\Delta\sigma-\Delta\sigma}{\frac{\Delta\sigma+2(\Delta\sigma)}{3}}=0,\ \ \Delta\sigma_3>0\\
&k_{\mathrm{IUT}}=k_{\mathrm{CTCT}}=3,\ \ \Delta\sigma_3=0\\
&k_{\mathrm{IUT}}=\frac{\Delta q}{\Delta p}=\frac{\Delta\sigma-(-\Delta\sigma)}{\frac{\Delta\sigma+2(-\Delta\sigma)}{3}}=-6,\ \ \Delta\sigma_3<0
\end{aligned}\right\} \tag{5}$$

$$\left.\begin{aligned}
&k_{\mathrm{KUT}}=\frac{\Delta q}{\Delta p}=\frac{\Delta\sigma-\Delta\sigma}{\frac{\Delta\sigma+2(\Delta\sigma)}{3}}=0,\ \ \Delta\sigma_3>0\\
&k_{\mathrm{KUT}}=k_{\mathrm{CTCT}}=3,\ \ \Delta\sigma_3=0\\
&k_{\mathrm{KUT}}=\frac{\Delta q}{\Delta p}=\frac{0-(-\Delta\sigma)}{\frac{0+2(-\Delta\sigma)}{3}}=-\frac{3}{2},\ \ \Delta\sigma_3<0
\end{aligned}\right\} \tag{6}$$

where $\Delta\sigma$ is the increment of stress; $\Delta\sigma_3$ is the increment of confining pressure; Δp and Δq are the average principal stress increment and the generalized shear strength increment, respectively; k_{CTCT}, k_{IUT}, and k_{KUT} represent the ratios of CTCT, IUT, and KUT, respectively. According to equations (5) and (6), k_{IUT}, k_{KUT}<0, it can be observed that the specimen has tensile failure (Fig.4 (a)), and $|k_{\text{IUT}}|>|k_{\text{KUT}}|$. Therefore the tensile failure in IUT is more significant. Furthermore, it can be observed that there is a significant relationship between the evolution characteristics of permeability and the k value: When k<0, the minimum value occurs at 50%-70% of the loading reaching the peak. When k>0, the minimum value occurs near the peak loading. Therefore, it can be considered that the magnitude relationship between α and 0 is related to the evolution of the permeability and the failure mode of limestone.

Furthermore, it can be observed that in CTCT and KUT, the specimens show a more obvious yield stage. Combined with the characteristics of k value, it can be considered that the yield of limestone is related to $|k|$. The larger the $|k|$ during the loading process, the more brittle the material shows. The smaller the $|k|$ is, the more likely the material is to show yield.

The mechanics and permeability parameters of limestone obtained from the three stress path tests are summarized and compared, and the results are shown in Fig.6. In the figure, μ represents Poisson's ratio, σ_{r} represents residual strength, and σ_{c} represents initial confining pressure. Among them, in test 3, due to σ_1 was kept before loading failure, it is difficult to define its peak stress, peak strain and other parameters, and it is also difficult to calculate parameters such as elastic modulus and Poisson's ratio. Considering that the residual strength can represent the long-term strength of the rock to a certain extent and has nothing to do with the definition of the peak value, the residual strength is mainly compared and analyzed in terms of mechanical properties. In terms of permeability, since the measured initial permeability and the minimum permeability do not show regularity, the reason is related to the discreteness of the sample, so the growth rate of the permeability in the growth stage is mainly analyzed.

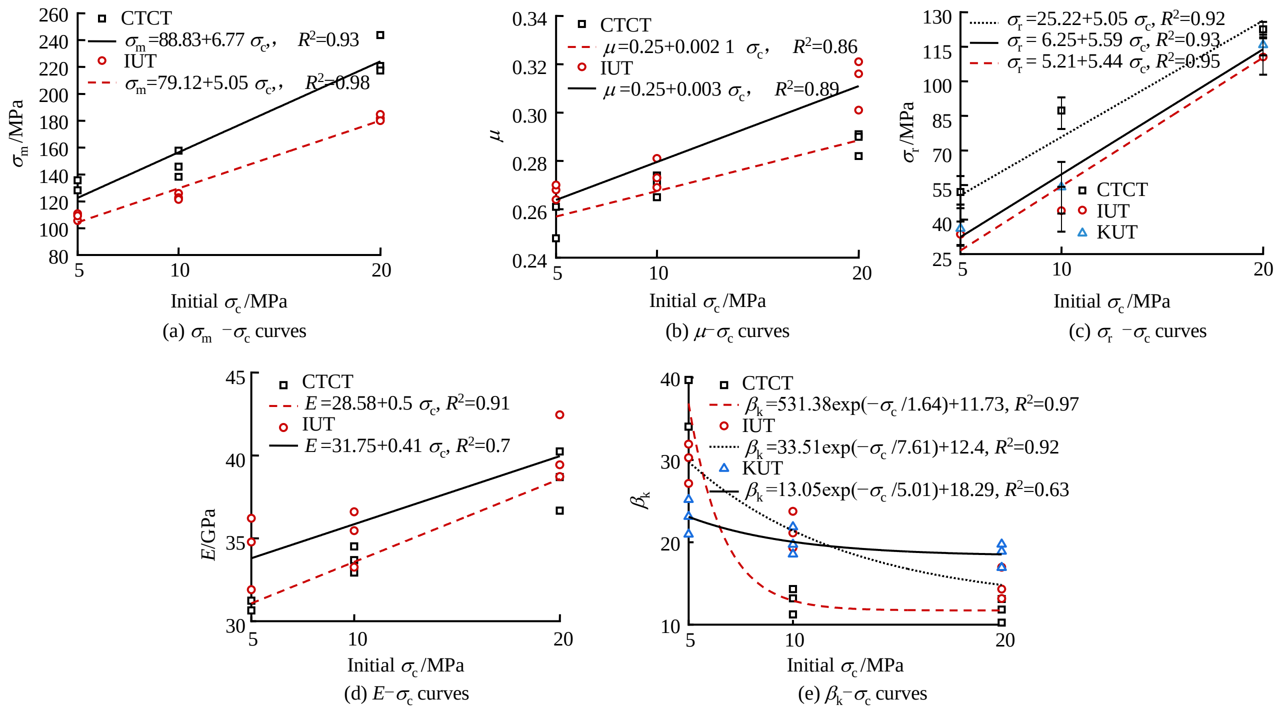

Fig.6 Performance parameters and fitting curves of limestone under three paths

It can be seen from Figs. 6 (a)-6(d) that under different stress paths, the relationship between the four parameters representing the strength and deformation characteristics of limestone: peak strength, residual strength, Poisson's ratio, deformation modulus and confining pressure are basically linear. Under the CTCT loading path, the strength of limestone is relatively high, but the deformation degree is relatively small. On the whole, there is a negative exponential relationship between permeability and confining pressure, which is consistent with the research results of Yang et al.[40] on rock characteristics under cyclic loading, and further indicates that the overall trend of permeability evolution is consistent under different stress paths.

To study the law of permeability growth of limestone, the growth rate of permeability β_k is defined:

$$\beta_{\text{k}} = \frac{k_{\text{r}} - k_{\text{p}}}{k_{\text{p}}} \tag{7}$$

where k_{r} is the permeability of the sample when it enters the participation stage; k_p is the permeability when the sample loading reaches its peak. As shown in Fig.6(e), under different stress paths, the growth rate of the permeability has a negative exponential relationship with the confining pressure. At the low confining pressure level (5 MPa), medium confining pressure level (10 MPa), and high confining pressure level (20 MPa), the stress paths corresponding to the maximum growth rate of the permeability are respectively: CTCT, IUT, KUT indicate that the evolution characteristics of the permeability performance of limestone is highly related to the in-situ stress level and stress state. In the excavation of shallow-buried roadways, more attention should be paid to the problems of water inundation and seepage. For deeply buried roadways, the ground stress level is relatively high, and the horizontal stress may be the large principal stress. The disturbance stress under this working condition should be studied by using the unloading test of the large principal stress.

The triaxial compression test is mainly to study the evolution characteristics of mechanics and permeability behavior of limestone during construction disturbance. For the long-term stability of roadway or tunnel in the construction process, it is also necessary to study through creep test.

3.2 Creep test

According to the study of Hao et al[12], the smaller the angle between the long axis of the tunnel and the direction of the principal stress, the stronger the roadway stability. When the horizontal stress is a large principal stress and the direction of the large principal stress is perpendicular to the direction of tunneling, the roadway stability is the weakest. This stress state should be similar to the stress path in test (3). In order to study the long-term stability of the roadway under this condition and the long-term stability of the rock mass as shown in Fig.1(b), the second type of creep test was conducted by unloading confining pressure.

3.2.1 Step loading creep test

Fig. 7 shows the results of the step loading creep test. According to the development of sample volume strain and permeability, the step loading creep test is divided into stages for analysis.

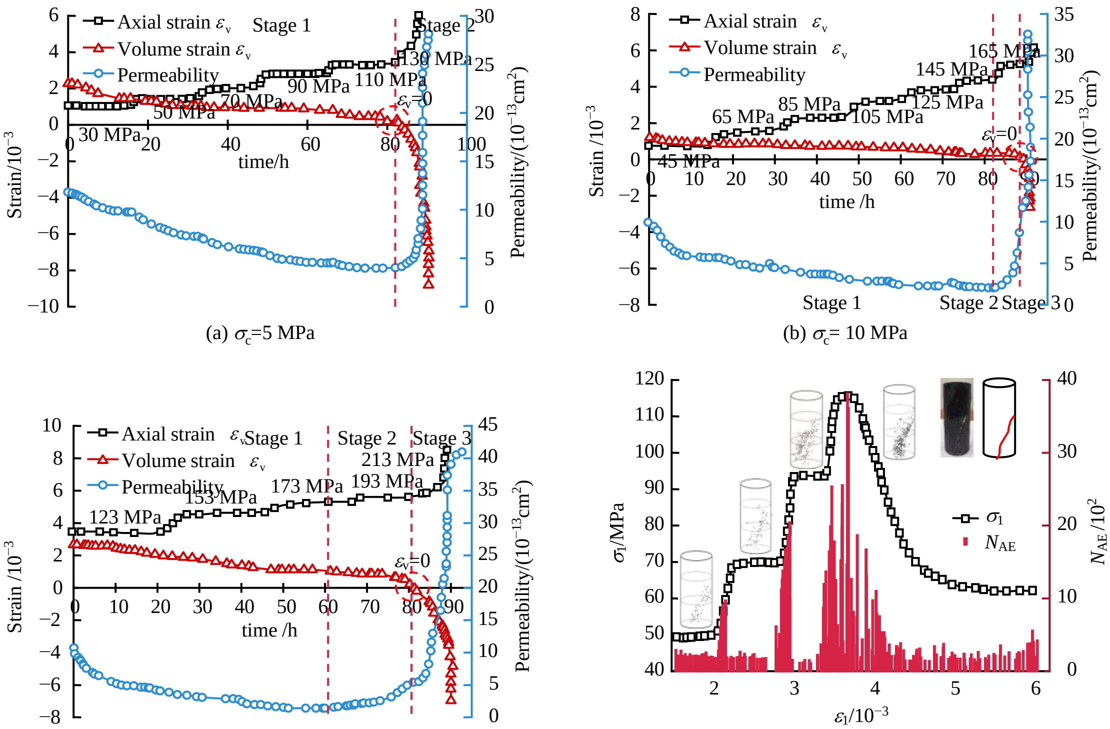

(a) σ_c=5 MPa (b) σ_c= 10 MPa (c) σ_c= 20 MPa (d) σ_c= 5 MPa，damage evolution

Fig.7 Results of stepped load creep test (σ_1 step loading)

When the confining pressure level is low, as shown in Fig.7(a), it is noted that volume strain ε_v reaching 0 and permeability reaching the minimum value are at the same loading time, so this is the boundary and divided into two stages: Stage (1) is the stage of low stress, and ε_v is constantly decreasing. In this stage, with σ_1 loading step by step, the permeability gradually decreases. In each stage of loading, the permeability goes through a diminution-stable change, and finally reaches the minimum value, entering the second stage. Stage (2) is the stage of failure stress, at which σ_1 loading reaches the last level and the specimen is damaged. In this stage, the permeability increases rapidly and the ε_v value increases continuously (negative value), indicating that the specimen is damaged and eventually destroyed.

With the increase of confining pressure level, as shown in Figs.7(b) and 7(c), at this time, sample ε_v drops to 0 in the permeability growth stage. Therefore, the test process is divided into three stages based on the two characteristics of minimum permeability and ε_v =0: There is a high stress stage between the low stress stage and the failure stress stage, in which ε_v >0 is still in the decreasing stage, but the permeability has begun to increase. This stage is more significant in the test of high confining pressure level, which indicates that water gushing is more likely to occur in the high ground stress environment in the long-term construction of underground mines.

It can be seen from Fig.7(d) that the number of AE events N_{AE} increases during the loading process of each stage of axial load, while in the subsequent creep process, N_{AE} returns to a lower level, indicating that the damage in the creep process mainly occurs during the loading process.

3.2.2 Unloading confining pressure creep test

The predetermined values of axial pressure under the two confining pressure levels are 119 MPa and 207 MPa, respectively.

The test results are shown in Fig.8. In the figure, ε_1 represents the axial strain. According to the boundary of the beginning of confining pressure unloading, the loading process is divided into two stages, that is, stage 1 is the conventional creep test, and stage 2 is the unloading confining pressure creep test. It can be clearly seen that both deceleration creep and constant velocity creep stages of limestone occur in stage 1. With the beginning of confining pressure unloading, limestone samples enter the accelerated creep stage, and the permeability increases rapidly. At the moment of confining pressure unloading, it can be observed that the N_{AE} increases rapidly and remains at a relatively high level in the subsequent process, as shown in Fig.8(c). In the test, shear failure was the main failure mode of the sample, as shown in Fig.8(d).

Compared with Fig. 7 and Fig. 8, it can be seen that under the creep test with the same initial confining pressure level, the failure rate of the specimen under the stress path of confining pressure unloading is faster than that under the stepped axial loading, which is consistent with the comparison results of the triaxial compression test.

The fitting analysis of various properties of limestone in the process of creep test 2 is carried out to study its evolution characteristics. The value of various properties of limestone samples in the test is related to the stress level (as shown in Fig.7). In order to better reveal the three-dimensional stress of rock mass, the equivalent principal stress p is used to characterize the stress level combined with the stress level set in the test.

The evolution characteristics of E_t under various stress levels is shown in Fig.9. E_t is the instantaneous elastic modulus of the rock at any given moment of loading, determined by the tangent slope of the stress-strain curve, and t is time. Consistent with the creep test process, it can be divided into two stages: In the first stage, the relationship between E_t and t is negative exponential; When the confining pressure starts to unload, it enters the second stage, and the relationship between E_t and t can be characterized by Boltzman's function. In the fitting process, in order to make the parameters in the formula have physical significance, note the negative exponential function, as shown

$$E_t = A\exp\left(\frac{-t}{T}\right) + B \tag{8}$$

where T is the parameter related to the shape of the fitted curve, and A, B are parameters related to the elastic modulus of limestone at different stages, determined through experiments.

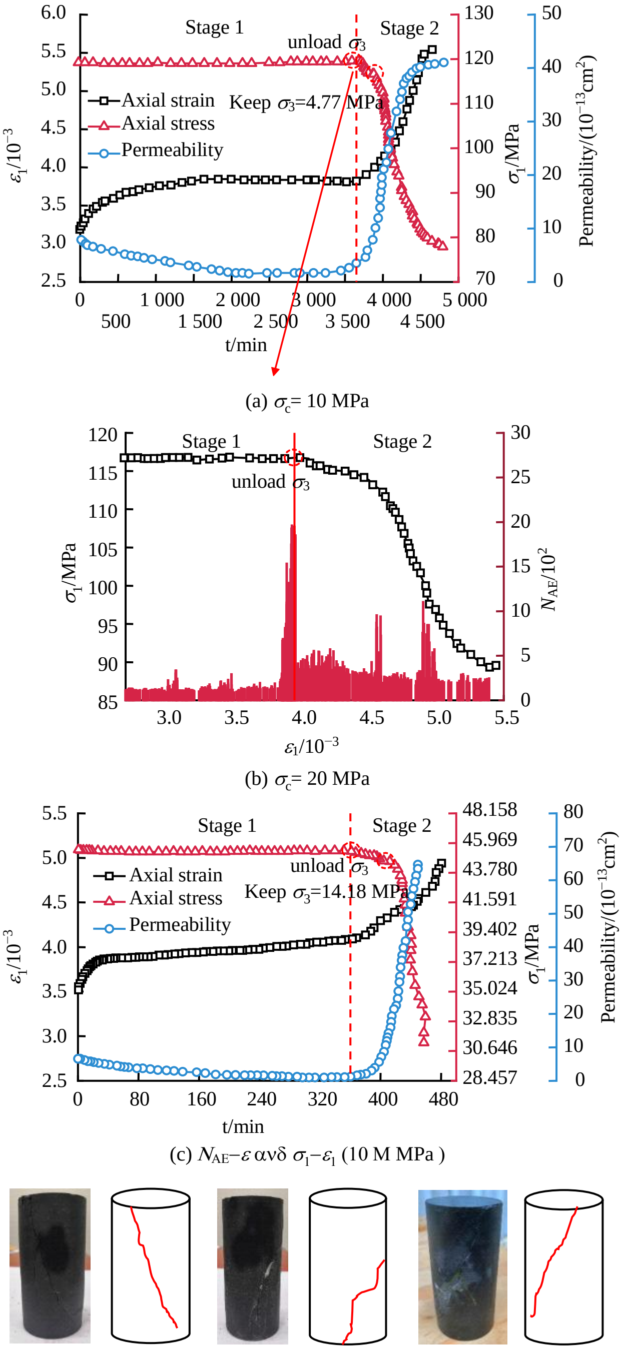

(a) σ_c= 10 MPa

(b) σ_c= 20 MPa

(c) N_{AE}–ε ανδ σ_1–ε_1 (10 M MPa)

(d) Failure mode

Fig.8 Unloading confining pressure creep test results (σ_3 unloaded)

Note that when t=0, the calculation result of equation (8) should be E_0, that is, the initial elastic modulus; When time enters the unloading confining pressure stage, the calculation result of equation (8) should be the final value of E at this stage, denoted as E_s, which can represent the long-term elastic modulus of the rock under creep state. Here we have: E_0=A+B; E_s =B. And since E_0 and E_s are functions of p. During the unloading stage of confining pressure, E_t is a function of both p and t, i.e. E_t =E (p, t). Therefore, Eq. (8) can be rewritten as

$$E(p,t)=(E_0-E_s)\exp\left(\frac{-t}{T}\right)+E_s \tag{9}$$

The fitting results are shown in Fig.9.

Similarly, in the unloading stage of confining pressure, the relationship between E_t and t can be expressed as:

$$E(p,t)=E_m+\frac{E_s-E_m}{1+\exp\left(\frac{t-t_s}{n}\right)} \tag{10}$$

where E_m is the final elastic modulus of the sample, which can represent the residual elastic modulus under long-term unloading confining pressure; and t_s is the horizontal coordinate of the maximum slope point. Considering that the deformation rate and damage rate of the sample begin to decrease gradually after the termination of unloading confining pressure, the moment when the confining pressure unloading is stopped is taken as t_s; and n is the characteristic parameter of the Boltzman's function, which represents the slope parameter of the curve. The fitting results are shown in Fig.9.

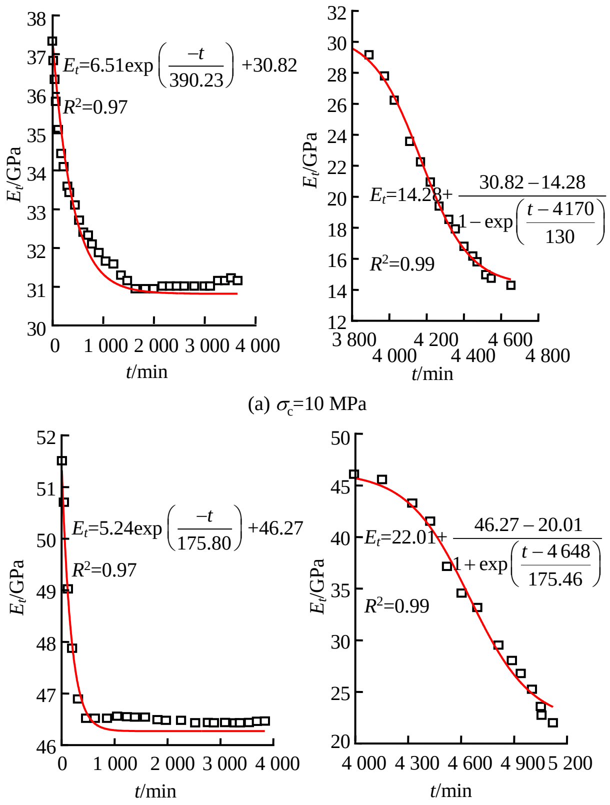

(a) σ_c=10 MPa

(b) σ_c=20 MPa

Fig.9 Time evolution law of elastic modulus

In this process, the damage variable D is defined as:

$$D=1-\frac{E_t}{E_0} \tag{11}$$

For the conventional creep stage, there are

$$D_1(p,t)=1-\frac{E(p,t)}{E(p,0)}=1-\left[\frac{E_s}{E_0}+\left(1-\frac{E_s}{E_0}\right)\exp\left(\frac{-t}{T}\right)\right] \tag{12}$$

where $D_1(p,t)$ is the damage variable in the conventional creep stage.

For the stage of unloading confining pressure, there are

$$D_2(p,t)=1-\frac{E(p,t)}{E_0}=1-\left\{\frac{E_m}{E_0}+\frac{E_s-E_m}{E_0\left[1+\exp\left(\frac{t-t_s}{n}\right)\right]}\right\} \tag{13}$$

where $D_2(p,t)$ is the damage variable during the unloading stage of confining pressure.

It should be noted that in the above fitting formula, the three parameters E_0, E_s and E_m are affected by the integrity and other properties of the specimen and the load stress level. Combined with the test results, the three parameters are linearly correlated with p.

$$E_0=0.407p+18.37, R^2=0.99 \tag{14}$$

$$E_s=0.405p+12.72, R^2=0.99 \tag{15}$$

$$E_s=0.24p+4.33, R^2=0.97 \tag{16}$$

As can be seen from Fig.7 and Fig.8, during the two creep tests, the samples underwent three stages of deceleration creep, constant velocity creep and accelerated creep. In the current creep constitutive models, such as Nishihara model and Burgers model, they can only reflect the deceleration creep and constant velocity creep state of rocks[46]. Therefore, in order to characterize the accelerated creep stage of limestone and minimize the complexity of the model, the Nishihara model is improved.

Considering that the relationship between ε and t in the accelerated creep state is approximately a quadratic function, the improved Nishihara model is shown in Fig.10. In the figure, η_1, η_2 are the fitting parameters representing the viscous characteristics of the model, k_1, k_2 are the fitting parameters representing the elastic characteristics of the model, and σ_s is the starting stress of the plastic element. Considering the three-dimensional stress state during unloading confining pressure, the starting condition of the plastic element is changed from σ_s to the generalized shear stress q_s, and the viscous element connected in parallel with the plastic element is replaced with a secondary viscous element to reflect the accelerated creep state when the generalized shear stress q is reaches, it enters an accelerated creep state. The constitutive relationship is

$$\sigma = \eta_2 \ddot{\varepsilon} \tag{17}$$

where σ is the stress; and $\ddot{\varepsilon}$ is the second derivative of strain ε with respect to time t, used to characterize the approximate quadratic relationship between ε and t in accelerated creep.

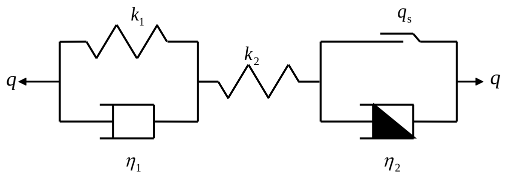

Fig.10 Improved Nishihara model

Finally, the constitutive equation of the improved Nishihara model is as follows:

$$\varepsilon = \begin{cases} \dfrac{p}{k_2\left[1-D_1(p,t)\right]} + \dfrac{p}{k_1\left[1-D_1(p,t)\right]} \cdot \\ \left[1-\exp\left(-\dfrac{k_1}{\eta_1}t\right)\right], \ q \leqslant q_s \\ \dfrac{p}{k_2\left[1-D_2(p,t)\right]} + \dfrac{p}{k_1\left[1-D_2(p,t)\right]} \cdot \\ \left[1-\exp\left(-\dfrac{k_1}{\eta_1}t\right)\right] + \dfrac{p}{\eta_2\left[1-D_2(p,t)\right]}t^2, \ q > q_s \end{cases} \tag{18}$$

The creep curve of staged loading was processed by using the Boltzmann superposition principle. According to the test results, the reliability of the model was verified, and parameter fitting was carried out through the LM method and the general global optimization algorithm of software 1stOpt. Some of the results are shown in Fig.11, and the corresponding model fitting parameters are presented in Table 1. It can be seen that the model has good reliability.

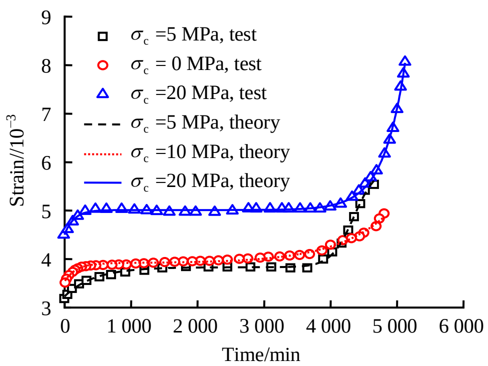

Fig.11 Reliability verification of creep models

Table 1 Fitting parameters for the creep constitute model

Test	σ_3/MPa	k_1/GPa	k_2/GPa	η_1/(GPa h)	η_2/(GPa h^2)	R^2
Creep test 2 (σ3 unloading)	5	31.92	280.11	7 274.56	19.11	0.99
	10	33.88	320.14	12 687.96	14.25	0.96
	20	35.19	381.56	11 873.33	11.22	0.97

4 Conclusions

In order to study the influence of mining disturbance on the stability of rock mass in front of coal mine face, a series of triaxial compression tests and creep tests with different stress paths were carried out to investigate the evolutionary characteristics of rock damage and permeability and their time-dependent mechanisms. The main conclusions are as follows:

(1) In the triaxial compression test, the performance evolution characteristics such as yield characteristics and permeability exhibited by limestone under different stress paths, as well as the relationship between permeability and loading conditions, have significant differences. Under the CTCT path, the minimum permeability point of limestone appears near the stress peak. With the increase of confining pressure, the minimum permeability point gradually approaches the stress peak point, and at the same time, limestone shows the yield characteristic. In the IUT and KUT, the minimum permeability formula is before the peak. When the confining pressure begins to be unload, the number of AE events E surges.

(2) The comparison and analysis of the parameters of limestone obtained from the triaxial compression test of the three paths show that the strength (including peak strength and residual strength) of limestone under the confining pressure unloading path is lower than that of the conventional stress path, while the parameters characterizing deformation (elastic modulus and Poisson's ratio) are higher. The relationship between the above strength parameters, deformation parameters and confining pressure is linear. There is a negative exponential relationship between the growth rate of permeability and confining pressure. At low confining pressure level (5 MPa), medium confining pressure level (10 MPa) and high confining pressure level (20 MPa), the stress paths corresponding to the maximum growth rate of permeability coefficient are as follows: CTCT, IUT and KUT, show that the evolution characteristics of limestone permeability has a great relationship with the ground stress level and stress state, and more attention should be paid to water inrush and seepage in shallow buried roadway excavation. For deep buried roadway, the ground stress level is high, and the horizontal stress may be large principal stress, so the disturbance stress under this condition should be studied by unloading test of large principal stress.

(3) In the creep test, the limestone samples in the step loading creep test and unloading confining pressure creep test, both show deceleration creep, constant velocity creep and accelerated creep processes. Most of the specimen damage occurs in the process of axial pressure step loading and confining pressure unloading, and the time required for specimen failure in the σ_3 unloading test is less than that in the axial pressure step loading test.

(4) The permeability evolution characteristics in creep

test is related to stress level. In the unloading confining pressure test, it gradually decreases in the creep process of the first stage, but rapidly increases in the unloading confining pressure creep process of the second stage. In the step load creep test, the permeability presents a periodic decreasing and stabilizing rule with the load of the main engine. At low confining pressure level, the permeability does not rise rapidly until the final failure horizontal load is loaded. At high confining pressure, the permeability increases earlier than the failure load.

(5) Based on the two stages of unloading confining pressure creep test, the characterization methods of the damage variables were proposed respectively. Considering that the relationship between ε and t in the accelerated creep stage is approximately a quadratic function, the Nishihara model was improved by introducing a new type of viscous element, and the reliability of the improved Nishihara model was verified according to the fitting of the test results.

References

[1] WANG Xin, XING An-kang, ZENG Zi-qing, et al. Experiment of shear mechanical properties of layered iron ore[J]. Rock and Soil Mechanics, 2025, 46 (4): 1039- 1048.

[2] ISRAR J, INDRARATNA B. Study of critical hydraulic gradients for seepage-induced failures in granular soils[J]. Journal of Geotechnical & Geoenvironmental Engineering. 2019, 145(7): 4019021-4019025.

[3] SUN Jie-hao, GUO Bao-hua, TIAN Shi-xuan, et al. Experimental study of direct shear failure characteristics of sandstone joints based on characteristic parameters of acoustic emission[J]. Rock and Soil Mechanics, 2024, 45 (Suppl.1): 167-177.

[4] LIU B C, XU S, HAO F, et al. Stress path and its application in energy geology: A review[J]. Geoenergy Science and Engineering. 2024, 241: 213095.

[5] WAGNER A C, SILVA J P D S, et al. Mechanical behavior of iron ore tailings under standard compression and extension triaxial stress paths[J]. Journal of Rock Mechanics and Geotechnical Engineering. 2023, 15 (7): 1883-1894.

[6] GUO J S, MA L Q, LIU Z G, et al. The influence of mining stress paths on rock damage and permeability[J]. Environmental Earth Sciences. 2024, 83(10): 1-20.

[7] GU L J, FENG X T, KONG R, et al. Excavation stress path induced fracturing mechanism of hard rock in deep tunnel[J]. Rock Mechanics & Rock Engineering. 2023, 56(3): 1779-1806.

[8] SUN Jie-hao, GUO Bao-hua, CHENG Sheng-jin, et al. Shear strength characteristics of rock-like joints in different control modes and unloading stress paths[J]. Rock and Soil Mechanics, 2024, 45 (7): 2061-2071.

[9] LI Y Q, ZHU Z M, HU R. Study on the effect of principal stress orientation on tunnel stability[J]. Journal of Sichuan University (Engineering Science Edition). 2012, 44(Suppl 1): 93-98.

[10] EBERHARDT E. Numerical modelling of three-dimension stress rotation ahead of an advancing tunnel face[J]. International Journal of Rock Mechanics and Mining Sciences. 2001, 38(4): 499-518.

[11] KARATELA E, TAHERI A, XU C, et al. Study on effect of in-situ stress ratio and discontinuities orientation on borehole stability in heavily fractured rocks using discrete element method[J]. Journal of Petroleum Science and Engineering. 2016, 139: 94-103.

[12] HAO X J, ZHANG Q, SUN Z W, et al. Effects of the major principal stress direction respect to the long axis of a tunnel on the tunnel stability: physical model tests and numerical simulation[J]. Tunnelling and Underground Space Technology. 2021, 114: 103993.

[13] FAN W C, TANG G D, HAN D Y, et al. An innovative test to study cracking behavior of fractured rock-like material under stepped excavation unloading[J]. Bulletin of Engineering Geology and the Environment, 2023, 82(12): 1-16.

[14] FERFERA F M R, SARDA J, BOUTÉCA M, et al. Experimental study of monophasic permeability changes under various stress paths[J]. International Journal of Rock Mechanics and Mining Sciences, 1997, 34(3-4): 121-126.

[15] LIU X R, ZHANG J L, ZHOU X H, et al. Damage-seepage evolution mechanism of fractured rock masses considering the influence of lateral stress on fracture deformation under loading and unloading process[J]. Rock Mechanics and Rock Engineering, 2024, 57(12): 1-27.

[16] ODA M O D D, TAKEMURA T, AOKI T. Damage growth and permeability change in triaxial compression tests of Inada granite[J]. Mechanics of Materials, 2002, 34(6): 313-331.

[17] MARTIN S S L D. Core disking and its relationship with stress magnitude for Lac du Bonnet granite[J]. International Journal of Rock Mechanics and Mining Sciences, 2010, 47(2):254-264..

[18] EBERHARDT E, STEAD D, STIMPSON B. Quantifying progressive pre-peak brittle fracture damage in rock during uniaxial compression[J]. International Journal of Rock Mechanics and Mining Sciences, 1999, 36(3): 361-380.

[19] CAI M, KAISER P K, TASAKA Y, et al. Generalized crack initiation and crack damage stress thresholds of brittle rock masses near underground excavations[J]. International Journal of Rock Mechanics and Mining Sciences, 2004, 41(5): 833-847.

[20] NIE B S, ZHANG H , LIU X F, et al. Experimental study on the mechanical stability and mesoscopic damage characteristics of coal under different mining disturbance rates[J]. Rock Mechanics & Rock Engineering, 2024(5): DOI:10.1007/s00603-023-03730-4.

[21] GONG F Q, ZHANG P L, XU L. Damage constitutive

model of brittle rock under uniaxial compression based on linear energy dissipation law.[J]. International Journal of Rock Mechanics & Mining Sciences, 2022, 160: 105273.

[22] LUO S, GONG F Q, LI L L, et al. Linear energy storage and dissipation laws and damage evolution characteristics of rock under triaxial cyclic compression with different confining pressures[J]. Transactions of Nonferrous Metals Society of China, 2023,.33(7): 2168-2182.

[23] NING J N, WANG J W, JIANG J J, et al. Estimation of crack initiation and propagation thresholds of confined brittle coal specimens based on energy dissipation theory[J]. Rock Mechanics & Rock Engineering, 2018, 51(1): 119-134.

[24] LI C, MO P Q, LI S C. Stability analysis of energy dissipation mechanisms in rocks surrounding circular opening[J]. Applied Mathematical Modelling, 2024, 127: 327-342.

[25] DIEDERICHS M S, KAISER P K, EBERHARDT E. Damage initiation and propagation in hard rock during tunnelling and the influence of near-face stress rotation[J]. International Journal of Rock Mechanics and Mining Sciences, 2004, 41(5): 785-812.

[26] YANG B C, ZHAO W, DUAN Y T. Critical damage threshold of brittle rock failure based on Renormalization Group theory[J]. Geomechanics and Geophysics for Geo-Energy and Geo-Resources, 2022, 8(5): 135.

[27] CHO S H, KANEKO K. Influence of the applied pressure waveform on the dynamic fracture processes in rock[J]. International Journal of Rock Mechanics and Mining Sciences, 2004, 41(5): 771-784.

[28] SONG M Y, HU Q T, LIU H H, et al. Characterization and correlation of rock fracture-induced electrical resistance and acoustic emission[J]. Rock Mechanics and Rock Engineering, 2023, 56(9): 6437-6457.

[29] LI Z Z, SUO J J, FAN J Y, et al. Damage evolution of rock salt under multilevel amplitude creep–fatigue loading with acoustic emission monitoring[J]. International Journal of Rock Mechanics and Mining Sciences, 2023, 164: 105346.

[30] FENG C C, WANG Z L, WANG J G, et al. Damage characteristics analysis and constitutive model establishment for deep rock considering pre-static loads and frequent dynamic disturbance[J]. Environmental Earth Sciences, 2023, 82(23): 559.

[31] FUJII Y, KIYAMA T, ISHIJIMA Y, et al. Circumferential strain behavior during creep tests of brittle rocks[J]. International Journal of Rock Mechanics & Mining Sciences, 1999, 36(3): 323-337.

[32] YU X, ZHANG T, YANG K, et al. Quantitative characterization of seepage behavior in rough fracture considering hydromechanical coupling effect: an experimental study[J]. Acta Geophysica, 2023, 71(5): 2245-2264.

[33] ZHANG W Q, ZHOU H T, GUO W H. Experimental study on seepage characteristics of fractured rock mass and its electrical response[J]. Journal of Hydrologic Engineering, 2019, 24(7): 04019017.1-04019017.10.

[34] SHI W H, YANG T H. A coupled nonlinear flow model for particle migration and seepage properties of water inrush through broken rock mass[J]. Geofluids, 2020, 2020(6): DOI:10.1155/2020/1230542.

[35] YANG F, LIN H X, SHEN L Y, et al. Water inrush mechanism of karst collapse column in coal seam floor based on a variable mass seepage mechanical model[J]. Geofluids, 2022,2022(1): DOI.org/10.1155/2022/8148203.

[36] GAO J Y, PENG S Y, CHEN G Q, et al. Coupled hydro-mechanical analysis for water inrush of fractured rock masses using the discontinuous deformation analysis[J]. Computers and Geotechnics, 2023, 15: 105247.

[37] ZHAO Y L, LIU Q, ZHANG C S, et al. Coupled seepage-damage effect in fractured rock masses: model development and a case study[J]. International Journal of Rock Mechanics and Mining Sciences, 2021, 144: 104822.

[38] WANG Y C, LIU Y, ZHAO N, et al. Investigation on the evolution mechanism of water and mud inrush disaster in fractured rock mass of mountain tunnel[J]. Geomatics, Natural Hazards & Risk, 2022, 13(1): 1780-1804.

[39] WANG J B, ZHANG Q, SONG Z P, et al. Microstructural variations and damage evolvement of salt rock under cyclic loading[J]. International Journal of Rock Mechanics & Mining Sciences, 2022, 152: 105078.

[40] YANG T J, WANG P Y, WANG S H, et al. Experimental study on shear-seepage coupling characteristics of single fractured rock mass under cyclic loading and unloading[J]. Rock Mechanics & Rock Engineering, 2022, 56(3): 2137-2156.

[41] BROWN E T. Rock characterization, testing & monitoring : ISRM suggested methods[M]. Oxford, UK: Pergamon Press, 1981.

[42] ASEMI F, LAKIROUHANI A, ZOHDI N A, et al. A new rock brittleness index based on crack initiation and crack damage stress thresholds[J]. International Journal of Geomechanics, 2024, 24(5): https://doi.org/10.1061/IJGNAI.GMENG-915

[43] XU R C, LI Z, JIN Y D. Brittleness effect on acoustic emission characteristics of rocks based on a new brittleness evaluation index[J]. International Journal of Geomechanics. 2022, 22(10): DOI.org/10.1061/(ASCE)GM.1943-5622.0002562.

[44] WANG W Q, FENG X T, WANG Q H, et al. 3D DEM simulation of hard rock fracture in deep tunnel excavation induced by changes in principal stress magnitude and orientation[J]. Journal of Rock Mechanics and Geotechnical Engineering. 2024, 16 (10): 3870-3884.

[45] DERSKI W, IZBICKI R, KISIEL I. Rock and soil mechanics[M]. Amsterdam: Elsevier Science, 2012: 739.

[46] TARIFARD A, GÖRÖG Á T P. Review of the creep constitutive models for rocks and the application of creep analysis in geomechanics[J]. Rock Mechanics and Rock Engineering. 2024, 57(10): 7727–7757.